Prediction of Surface Deformation for Open Cast Mine Based on Pit Wall Prisms Monitoring Dataset*

[1]I. Yakubu, [1]Y. Y. Ziggah and [2]F. Osei
[1]University of Mines and Technology, Box 237, Tarkwa, Ghana
[2]Postgraduate Candidate, University of Mines and Technology, Box 237, Tarkwa, Ghana

Yakubu, I., Ziggah, Y. Y. and Osei, F. (2024), "Prediction of Surface Deformation for Open Cast Mine Based on Pit Wall Prisms Monitoring Dataset", *Ghana Mining Journal,* Vol. 24, No. 1, pp. 27-40.

Abstract

This paper explores the application of Artificial Intelligence (AI) techniques for predicting pit wall deformation in open-cast mining operations. Four AI models, including the Patient Rule Induction Method (PRIM), Radial Basis Function Neural Network (RBFNN), Back Propagation Neural Network (BPNN), and Group Method of Data Handling (GMDH), were developed and evaluated to estimate pit wall deformation for three different monitoring locations designated as Prisms 1, 2 and 3. The AI models were statistically evaluated using dimensioned error indicators such as Mean Square Error (MSE), Root Mean Square Error (RMSE) and Mean Absolute Error (MAE). The coefficient of determination (R^2) was also used for the model's performance evaluation. The study concluded that for the Prism 1 monitoring point, the BPNN was the most suitable for predicting the pit wall deformation. However, for Prisms 2 and 3, the RBFNN demonstrated superior performance, with minimal errors and high R^2 scores, making it a suitable choice for deformation prediction. GMDH exhibited fair results, while PRIM produced significant prediction errors, rendering it less suitable for pit wall deformation estimation. In general, the study findings suggest that AI techniques can significantly enhance and automate the deformation prediction process in open-cast mining, offering opportunities for improved safety and operational efficiency.
.

Keywords: Deformation, Open Pit Mine, Artificial Intelligence

1 Introduction

Surface deformation refers to changes in the shape, height, and/or location of the Earth's surface caused by natural or anthropogenic forces. It is a frequent mining phenomenon that may occur in both open-pit and underground mines. Removing large amounts of rock and soil is the primary cause of surface deformation in open-pit mining. As the material is taken from the earth, the underlying rocks and soil can shift and settle, resulting in subsidence or sinking of the ground surface. This might result in surface cracks, fractures, and uneven ground. In rare cases, subsidence can spread outside the mining zone, damaging nearby infrastructure and communities. Another factor that leads to surface deformation in open pit mining is heavy machinery and gear use. By exerting vibration and impact on the ground surface, these devices can cause soil compaction and settling.

Moreover, excavation can cause the surrounding rock and soil to become unstable, resulting in landslides and rock falls. Disposing of garbage and exploiting mineral reserves might alter the natural hydrological cycle of the area. This can cause changes in groundwater levels and flow, exacerbating surface deformation. Geological factors such as the presence of faults, fractures, and weak zones in the ground can also induce surface deformation in open-cast mines.

Surface deformation can have several consequences for the surrounding environment. It can, for example, alter the land's topography and drainage patterns, causing changes in water and nutrient distribution. This may affect local plant and animal populations, potentially leading to habitat loss and a decline in biodiversity. It may also cause soil erosion, which may cause sedimentation in nearby streams and impact aquatic habitats. Surface deformation could influence the region's availability and quality of water supplies due to pollutants or toxic substances released during the deformation phase. Subsidence, for example, could demolish buildings and infrastructure, resulting in harm or death.

With regard to mine subsidence, the release of dust and other pollutants can also influence air quality. Hence, there is a need for continual monitoring of the stability and deformation of an open pit mine's walls. The primary purpose of pit wall monitoring is to guarantee the safety of mine personnel and equipment by identifying any possible wall instability or movement. Moreover, pit wall deformation can also socially influence the communities around it. For example, safety risks and environmental consequences may cause dread and worry among nearby residents, potentially leading to social conflict between mining companies and local communities. Therefore, the stability of steep slopes in open pit mines is a serious safety concern.

Many approaches for open pit slope monitoring have been used in recent years. Conventional slope monitoring systems combine geotechnical sensors and surveying tools. However, newer systems use new approaches ranging from permanent GPS stations to

*Manuscript received April 29, 2024
Revised version accepted July 05, 2024
https://doi.org/10.4314/gm.v22i1.1

radar interferometric data. Because of the dependability and precision provided by surveying equipment, surveying techniques are nearly always utilised in open pit mines, independent of additional sensors that may be used in conjunction. Robotic total stations are now frequently utilised as the principal measurement equipment in conjunction with meteorological sensors and interfaced with computers and wireless communication capabilities to transfer data to a processing centre.

Predicting the projected duration of slope collapse is crucial in open pit slope stability management since it outlines the necessary procedures to be taken. It is vital to know when to evacuate, but it is also helpful to know ahead of time if a certain slope is about to collapse or if the deformations detected are unlikely to result in collapse. Knowing this information beforehand allows a mine to plan and implement corrective actions, such as schedule adjustments, slope angle changes, and buttresses, to decrease economic and safety concerns (Zhang *et al.*, 2017).

The mining sector contributes immensely to the development and economic growth of countries. In Ghana, the said sector was regarded as one of the priority areas of the country's Economic Recovery Programme (ERP) in 1983 due to the large production of gold, placing Ghana as the second largest gold producer in Africa and ninth in the world. Over the years, mining has evolved along with technology, and several methods of exploiting these minerals have been established to enhance production and make mining safer. As much as mineral resources have contributed immensely to the world's socioeconomic development, they have also caused enormous geological and security problems in mining areas (Zhou *et al.*, 2021). For example, surface subsidence emanating from mining has caused regional disasters such as ground fissure, collapses, and pitfalls, which severely threaten the safety of production and, therefore, raise several questions about the ecology of the environment (Yakubu *et al.*, 2018; Huang *et al.*, 2019; Dong *et al*., 2020). Dangers attributed to mining deformation are always crucial in mining safety production.

Over the last 100 years, the failure of mine tailings dams has been a primary public concern and a source of high liability risk for the mining industry. The earliest tailings dam failure was recorded in 1915 at Agua Dulce in Chile, where overflow due to heavy rains resulted in the dam's collapse and the release of 180 000 cubic meters of copper tailings into the environment. On a serious note, the most catastrophic tailings dam failures happened from 1990 to 2010. Out of the 67 tailings dam failures from 1940 to 2010, 52 occurred between 1990 and 2010, when modernisation was at its peak. According to dam committee reports and government accounts, these losses can all be attributed to a failure to follow standard operating procedures and policies, such as deformation monitoring on the facilities (Bowker and Chambers 2015). To achieve mine sustainable development, there is a need to monitor and analyse land deformations caused by mining activities, determine the settlement range, and control the occurrence of geological hazards. This provides practical help and experience as a reference for comprehensive management of the subsidence area (Huang *et al.*, 2019).

With the continuous upgrade in surveying and mapping technologies, there has been substantial progress in monitoring mine surface deformations (Zhou *et al*., 2021). Traditional and ground-based technologies such as Robotic Total Station (RTS), Synthetic Aperture Radar (SAR), and Synthetic Aperture Radar Interferometry (InSAR) have been broadly used by the geoscientific community for monitoring the stability of open cast pit walls (Dong *et al*., 2020). The introduction of the Continuous Operating Reference System (CORS), Wide Area Augmentation System (WAAS), and Real Time Kinematics (RTK) are some new developments for improved geodetic-based monitoring.

Even though these enumerated geodetic measurements can accurately measure three-dimensional surface deformation, the computational process is not straightforward. Earlier studies (Miima and Niemeier, 2004; Kalkan and Chopra, 2010; Osasan and Afeni, 2010; Kutterer, 2010; and Zhou *et al.*, 2021) have suggested numerical and statistical techniques for predicting structural deformations. However, these methods had limitations, considering the non-linearity and complex nature of structures associated with open-pit mines. Initial boundary conditions are also needed for the full implementation of the methods. Therefore, to automate the computational process for quick decision-making, proper planning, and management of safety, it is imperative to use a technique that can model the continuous surface and handle appropriately the dynamic nature of deformation (Miima and Niemeier, 2004; Kutterer *et al*., 2010; Zhou *et al.*, 2021).

Consequently, scholars (Gourine *et al*., 2012; Du *et al*., 2013; Cheng and Xiong, 2017; Miao *et al.*, 2018; Sunwen *et al*., 2019) have relied on the use of Artificial Intelligence (AI) techniques to solve multivariate nonlinear prediction problems in deformation studies in dams, viaducts, and bridges, among others. A review of these studies indicates that the AI methods can serve as a reliable substitute for the traditional numerical and statistical deformation modelling methods. This is due to their high attenable prediction accuracy, low computing time, and self-adaptive nature.

1.1 Artificial Intelligence Methodologies

Artificial intelligence (AI), in general, is the study and development of intelligent agents, where an intelligent agent is a system that examines its environment and takes actions to maximise its chances of success (Russell and Norvig 2003). Many real-world problems need the agent to work with incomplete or confusing facts (Negnevitsky, 2005). Using AI techniques has many advantages over traditional development and implementation strategies (Russell and Norvig, 2003; Negnevitsky, 2005). These include quick access to collected knowledge (e.g., knowledge-based systems), easy-to-implement prototypes without deep expert knowledge (e.g., artificial neural networks (ANNs)), or systems that can learn (e.g., evolutionary optimisation algorithms).

Given the enumerated benefits, a variety of AI methodologies have been employed to anticipate mine slope surface deformation. For example, ANN, which is a type of machine learning composed of interconnected nodes that process incoming data and forecast output, has been employed for predicting deformation (Li *et al*., 2019). Support vector machine (SVM) is another machine learning technique that has been utilised for prediction problems (Jia *et al*., 2019). The SVM works by selecting the best boundary or hyperplane for classifying data points. Random Forest, another ensemble learning technique that predicts by mixing many decision trees, has also been considered.

Convolutional neural network, a type of deep learning technique frequently used for image recognition, is used to estimate mine slope surface deformation by processing input data hierarchically, learning characteristics at various sizes, and making predictions based on those features (Xu and Qiu, 2021). Long Short-Term Memory Network (LSTM) is a recurrent neural network designed to handle sequential data like time series data, which can be used to anticipate mining slope values in the future (Zhang *et al*., 2020).

Some of the AI Methods Applied in this Research includes; Patient Rule Induction Method, Group Method of Data Handling, Back Propagation Neural Network, and Radial Basis Function Neural Network.

1.1.1 Patient Rule Induction Method

The Patient Rule Induction Method (PRIM) is a data mining technique for identifying regions in a dataset where a certain outcome is more likely to occur. This method is especially useful when several predictors or factors in the data might influence the conclusion. The PRIM technique separates the data into smaller regions or subsets, each representing a potential collection of elements or predictors associated with a certain result. The technique then repeatedly looks for the subset with the highest proportion of desired outcomes and repeats this approach until a stopping condition is met.

The PRIM can be used to evaluate mine surface deformation data and develop rules that characterise the circumstances or causes related to the deformation. This can help predict and manage future deformation problems in mining operations. The following describes the computational procedures of PRIM for surface deformation.

Step 1: Initial Area construction
The procedure begins by constructing an initial area that includes all the mine surface deformation data.

Step 2: Candidate Subset Generation
A subset of the beginning region is selected using a set of criteria designed to optimise the proportion of deformation events. Typically, this is performed by selecting a set of events or attributes relevant to mine surface deformation, such as geological features, mining operations, or weather conditions.

Step 3: Quality Control
A set of criteria, such as the proportion of deformation occurrences or the size of the subset, determines the quality of the candidate subset. If the subset meets the quality standards, it is acknowledged as a new region. The method returns to step 2 if the candidate subset is rejected.

Step 4: Stopping Criterion
The algorithm repeats stages 2 and 3 until a stopping condition is fulfilled. The stopping condition might be a set number of iterations, a degree of precision or accuracy, or a quality threshold (Miao *et al*., 2018)

1.1.2 Back Propagation Neural Network

The Backpropagation Neural Network (BPNN) is a type of ANN that trains the network to predict an output variable based on a collection of input variables using supervised learning. The technique has been extensively used in image recognition, audio recognition, and natural language processing applications. The BPNN comprises three layers: an input layer, one or more hidden layers, and an output layer. Each layer has a collection of nodes or neurons that process the input data. The connections between nodes are weighted, and these weights are adjusted throughout training to increase prediction accuracy.

The BPNN training algorithm is divided into two stages: forward and backpropagation. In the forward propagation phase, the input data is received by the input layer and sent through the network, and the outputs are generated based on the weights of the connections between the nodes. The error between the expected and actual outputs is computed during the backpropagation phase, and the weights are modified to minimise this error. This method is continued until

the prediction error is reduced to an acceptable level (Duddu *et al.*, 2020; Samantaray and Sahoo, 2020; and Zhu *et al.*, 2021)

1.1.3 Group Method of Data Handling

The Group Method of Data Handling (GMDH) is a data-driven modelling technique commonly used to solve regression and classification problems. The GMDH method employs a mix of linear and nonlinear functions to represent the data. The linear functions are used to approximate the data's global trend, while the nonlinear functions capture the data's local changes (Zhang *et al.*, 2017). The method is an iterative and adaptive method for dealing with high-dimensional and complicated data and has several uses, including engineering, finance, and medical application.

The GMDH method employs a divide-and-conquer strategy to learn a model from data, repeatedly picking and combining parameters that reduce error (Amiri and Soleimani, 2021). The GMDH method begins with a collection of candidate features and uses a forward selection procedure to select the subset of input features that minimises error. The algorithm picks the feature that minimises the error in each stage of the forward selection when paired with the previously picked characteristics. This procedure is iterated until the required degree of accuracy is obtained or the number of chosen parameters reaches a predetermined threshold.

1.1.4 Radial Basis Function Neural Network

The Radial Basis Function Neural Network (RBFNN) is a type of ANN that models the relationship between input and output variables using radial basis functions. RBFNN is widely utilised in a wide range of applications, including pattern recognition, time-series prediction, and control systems. There are three layers in the RBFNN: an input layer, a hidden layer, and an output layer. The input layer receives the input data, while the hidden layer uses radial basis functions to accomplish the nonlinear mapping. The output layer generates the anticipated output based on the weighted sum of the hidden layer's outputs.

The prototypes, which are typical samples of the input data, are at the center of the radial basis functions. The radial basis function computes the distance between the input data and the prototypes and feeds it into the activation function. The activation function transforms the distance into a nonlinear output, which is then transferred to the output layer. A learning method, such as the unsupervised K-means clustering algorithm or the supervised backpropagation algorithm, determines the weights and centres of the radial basis functions. A trial-and-error or validation method is often used to determine the number of radial basis functions (Xu *et al.*, 2012; Mostajeran and Hosseini, 2023). The RBFNN offers various benefits, including the ability to handle nonlinear connections, a short training period, and resistance to noise and outliers.

With the enumerated potential benefits of using AI technology in deformation studies, the current research seeks to evaluate different the four (4) AI models to predict open-cast mine wall deformation, using Mine XYZ ltd open pit in southern Ghana as a case study.

2 Study Area

The study area is a large-scale gold mining company located in the southern part of Ghana (Figure 1). For the purposes of this research, the mining firm will be known as Mine XYZ Ltd. Some of the large-scale gold mining companies are; AngloGold Ashanti (Ghana) Ltd (Obuasi and Iduaprim), Gold Fields Ghana Ltd (Tarkwa and Damang), Newmont Ghana Gold Ltd (Keyansi and Akyem), Perseus Mining (Ghana) Ltd (Ayanfuri), Asanko Gold Mine Ltd (Amansie West), Chirano Gold Mines Ltd, Adamus Resources Limited (Teleku Bokazo,Nzema), Golden Star Ltd (Prestia/Bogoso and Wassa).

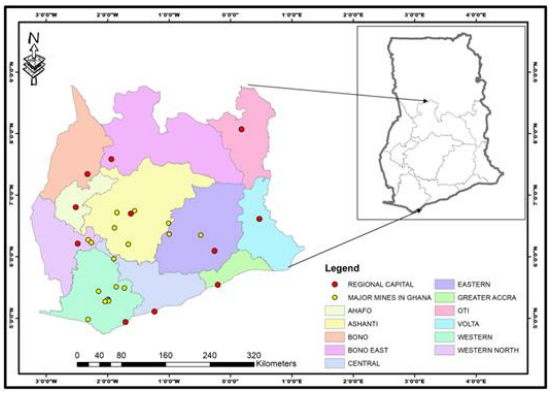

Fig. 1 Map of Southern Ghana Showing Large-Scale Gold Mining Areas

3 Resources and Methods Used

3.1 Data Description and Division

The primary data set used for the research was obtained using the Leica robotic total station. The instrument is set on 3-dimensional geodetic control to first measure a permanent back site prism mounted on a permanent control and to three prisms point locations mounted on the Mine X pit walls. At a specific epoch, one hundred twenty-nine (129) mine grid coordinates (Easting, Northing, Elevation) were measured on each prism mounted on the pit walls. These data were divided into training and testing sets of 70% and 30%, respectively. The data division was based on the hold-out-cross-validation approach, which has been used in similar mining predictive models, such as blast-induced ground vibration (Arthur *et al.*, 2019). Using this popular method, the training set used in designing

the predictive model requires a larger proportion of the total observations; hence, the training sets for each prism were apportioned 90, representing 70% of the entire 129 coordinates observed. The remaining 39, representing 30% of the 129 data set, were used as the testing set to verify the prediction accuracy of the optimum trained model for each prism. Equation (1) was used to calculate the displacement (deformation) based on the observed mine grid coordinates (Easting, Northing, and Elevation).

$$D = \sqrt{(HM)^2 + (VM)^2} \quad (1)$$

The *HM* and *VM* were computed using Equations (2) and (3).

$$HM = \sqrt{(\Delta E)^2 + (\Delta N)^2} \quad (2)$$

$$VM = \sqrt{(Z_i - Z_1)} \quad (3)$$

where *D* is the displacement, *HM* is the Horizontal Movement, and *VM* is the Vertical Movement. The ΔE and ΔN are the cumulative differences in the Eastings and Northings, Z_i, and Z_1 are the base elevation and the subsequent elevations, respectively.

The software used in building the AI models was MATLAB 2016(a). All codes and algorithms for building and evaluating the models were run with the software.

3.1.1 Deformation Analysis

Deformation analysis involves determining whether point displacements are substantial. To ascertain the significance of these displacements, they are juxtaposed with their respective 95% confidence intervals or ellipses (Bird, 2009). This method evaluates the computed displacement magnitude against the 95% confidence interval to verify if notable movement occurred between observation epochs. Should the calculated displacement magnitude exceed the 95% confidence interval, it indicates a significant movement. However, should the computed displacement be less than the 95% confidence interval, no displacement has occurred, and the displacement could be attributed to measurement error (Okiemute *et al*., 2018). The equation for computing the confidence interval is provided in Equation (4).

$$CI = 1.96\sqrt{\sigma_{k+1}^2 + \sigma_k^2} \quad (4)$$

where σ_{k+1}^2 is the standard error of the position $K + 1$ epoch, and σ_k^2 is the standard error for the previous epoch K.

3.2 Methods Used

Figure 2 provides a flow chart on the various stages employed in developing the AI models. Firstly, the mine grid coordinates (E, N, and Z) served as the input variables in the AI models evaluated, and the computed displacement (D) served as the target or output variable. Due to different data variability in the E, N, and Z, data normalization was performed. Its significance is to avoid larger values having influence on the smaller recorded data and slowing the AI algorithm to reach convergence. The normalized input data sets were then fed as input into the AI methods with *D* as the target. The supervised learning technique was used for all the AI models utilised in this study for predicting *D*. The next stage was to train the model of which network configuration of the controlling parameters was adjusted to achieve better model prediction. The selected optimum trained model was tested using the testing data. The essence is to independently assess or verify the validity of the trained model. A model is selected as optimum when the loss function is within the acceptable tolerance value. In this study, the Root Mean Square Error (RMSE) was used as the criterion for deciding the optimum trained model. A model with the least testing and training RMSE value among candidate results from the model is chosen as the best. The subsequent sections present a detailed account of the methods applied.

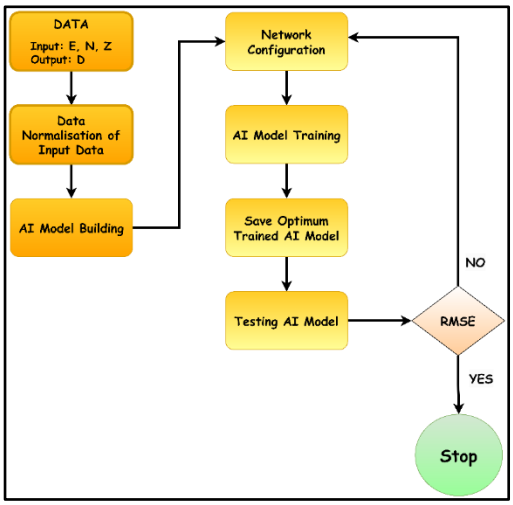

Fig. 2 Stages of the AI Modelling

3.2.1 Group Method of Data Handling

GMDH networks automatically calculate the most crucial input variables, the number of layers, the number of neurons in hidden layers, and the ideal model structure. Hence, the network is made up of neurons that are active and self-organised. The GMDH network learns inductively and attempts to construct a polynomial model function that would lead to the least error between the predicted value and expected output (Srinivasan, 2008). To characterize the intricate nonlinear interactions between a system's input and output parameters, GMDH employs a multilayer network of the second order of the Kolmogorov-Gabor polynomial (Arthur *et al*., 2019) expressed in Equation (4).

$$y = a_0 + a_1 x_i + a_2 x_j + a_3 x_i x_j + a_4 x_i^2 + a_4 x_j^2 \quad (4)$$

where x_i and x_j are the input variables, y is the predicted output, a is the vector of the coefficient of the polynomial function.

As part of the computational process, the GMDH constructs layer after layer of intricate links (or connections) made up of each term of a polynomial. Regression techniques, both linear and nonlinear, are used to construct these polynomial terms. The input layer is the only layer in the beginning where regression analysis of the input variables is performed, and the best candidates are then selected to form the first layer. The values from the first layer and input variables are used to compute regressions to produce the second layer. As a result, the method creates polynomials of polynomials where only the best is selected. This procedure continues until a predetermined selection criterion is satisfied (Srinivasan, 2008). In this research, the input variables are the E, N, and Z coordinates collected from the mine, and the output variable is the 3D displacement (D) obtained from the collected data.

3.2.2 Radial Basis Function Neural Network

As illustrated in Figure 3, the RBFNN is a three-layered feed-forward neural network comprising an input, a hidden layer, and an output layer. Under this study, the input layer consists of the E, N, and Z coordinates and D as the target. The hidden layer accepts data from the input layer. Each hidden layer has an activation function (radial basis functions) that models the non-linearity of the input data. The activation function used in the hidden layer for this study is the Gaussian type. The output layer has a linear combinatory function that linearises data from the hidden layer to obtain the 3-dimensional displacement (D) required.

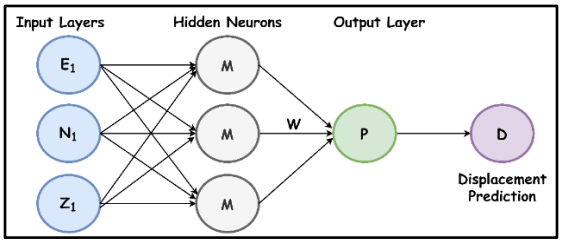

Fig. 3 RBFNN Architecture

3.2.3 Back Propagation Neural Network

Figure 4 shows the architecture of BPNN which comprises an input layer, a hidden layer, and an output layer. The input layer, which consists of weighted training or testing sets, is processed in the hidden layer by the nonlinear hyperbolic tangent activation function. Even though there are numerous activation functions, such as the sigmoid function, rectified linear unit, and softplus (Apraku *et al*., 2022), the hyperbolic tangent activation function was chosen due to the efficient and effective results it has produced in similar deformation predictive models.

The 3D-displacement output generated from the hidden layer serves as inputs for the output layer, which contains existing displacement values as determined from the primary data via a linear activation function to generate a final network.

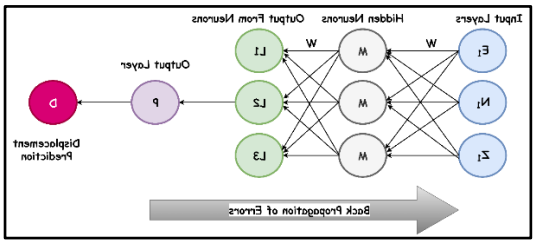

Fig. 4 BPNN Architecture

3.2.4 Patient Rule Induction Method

The PRIM is a tool that is used to find a region of interest using a discrete sample and then define it in an interpretable way using a set of hypercubes (or boxes). PRIM is used for locating areas of an outcome space that are of particular interest, which it does by reducing the data size incrementally by small amounts in an iterative process. Thus, candidate boxes are generated, and these boxes represent incrementally smaller sets of data. Each box removes a portion of the data based on the levels of a single input variable.

For each candidate box, the relative improvement is achieved through the peeling strategy (–i.e., a peeling step successively strips the generated box in smaller strips till it becomes smaller/apparently impossible to strip) where the number of outcomes of interest inside the box is calculated. The candidate box with the greatest improvement is selected. Pasting is also one algorithm in the improvement step as it readjusts the outcomes of the peeling strategy. The procedure for pasting is basically the inverse of the peeling procedure. Starting with the peeling outcome, the current box is enlarged by pasting along its boundary 'small' strips. The data in the selected candidate box replaces the starting data, and the process is repeated until a stopping criterion is met.

3.3 Model Evaluation

Model evaluation is the process of using different evaluation metrics to understand a machine learning model's performance, as well as its strengths and weaknesses. This is important because it provides the opportunity to assess the efficacy of a model. In this study, the following statistical evaluators were used for the model performance evaluation:

i. R-squared (R^2): R-squared is a measure of how well the predicted values of the model fit the actual data. It represents the proportion of variance in the target variable that the model can explain. R^2 ranges from 0 to 1, with higher values indicating a better fit. An R^2 value close to 1 indicates that the model explains a large portion of the variance in the data, while a value close to 0 indicates a poor fit. The mathematical equation for finding the coefficient of determination (R^2) is expressed in Equation (5):

$$R^2 = 1 - \frac{RSS}{TSS} \quad (5)$$

where, RSS is the sum of squared residuals (the sum of the squared differences between the predicted and actual values), and TSS is the total sum of squares (the sum of the squared differences between the actual values and the mean of the actual values).

ii. Root Mean Squared Error (RMSE): RMSE is a measure of the average error between the predicted and actual values. It is calculated by taking the square root of the mean of the squared differences between the predicted and actual values. RMSE is commonly used to evaluate the accuracy of a model's predictions, with lower values indicating better accuracy. The mathematical formula is expressed in Equation (6) as:

$$\text{RMSE} = \sqrt{\frac{\sum_{i=1}^{N}(x_i - \hat{x}_i)^2}{N}} \quad (6)$$

where, N is the number of samples, $\hat{x}_i$ is the predicted value, and x_i is the actual value.

iii. Mean Absolute Error (MAE): As expressed in Equation (7), MAE measures the average absolute difference between the predicted and actual values. It is calculated by taking the mean of the absolute differences between the predicted and actual values. MAE is another commonly used indicator of prediction accuracy, with lower values indicating better accuracy.

$$\text{MAE} = \frac{\sum_{i=1}^{n}|y_i - x_i|}{n} \quad (7)$$

where, y_i is the predicted value, x_i is the true value, and n is the number of data points.

iv. Mean Absolute Percentage Error (MAPE): MAPE is a measure of the percentage difference between the predicted and actual values. It is calculated by taking the mean of the absolute percentage differences between the predicted and actual values and expressing it as a percentage. MAPE is useful for evaluating the prediction accuracy in terms of percentage error, which can be helpful in certain applications where relative errors are very important. It is expressed in Equation (8) as:

$$\text{MAPE} = \frac{1}{n}\sum_{t=1}^{n}\left|\frac{A_t - F_t}{A_t}\right| \quad (8)$$

where, n is the number of times the summation iteration happens, A_t is the actual value and F_t is the forecasted value.

These indicators provide different perspectives on the performance of AI prediction models and can be used in combination to get a comprehensive evaluation. It is important to interpret these indicators in the context of the specific problem and data at hand and consider the trade-offs between different metrics based on the application requirements. Additionally, model evaluation should be performed using appropriate validation techniques, such as cross-validation, to ensure reliable and robust results.

4 Results and Discussion

4.1 Comparison between Displacements and their Corresponding 95% Confidence Interval

Figures 5 to 7 presents the 3D displacement magnitudes for the monitoring prisms and their respective 95% confidence interval. The displacements for the monitoring prisms (Prism 1, Prism 2, and Prism 3) were computed and compared with their respective 95% confidence intervals. This undertaking was to ascertain if the computed 3D displacements were indeed wall movements or just measurement or instrument errors. From the figure it can be established that there is movement in the mine wall as most of the computed 3D displacement were greater than the 95% confidence interval.

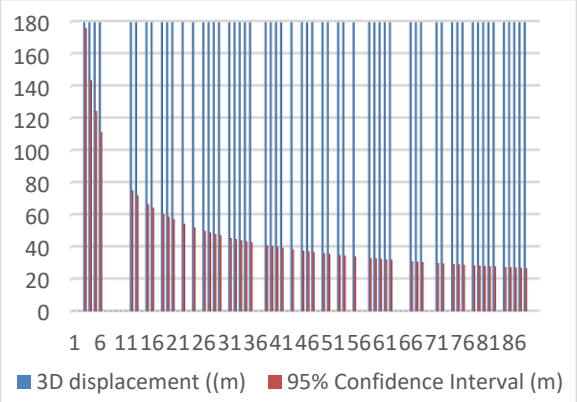

Fig. 5 3D Displacement and their respective Confidence 1ntervals for Prism 1

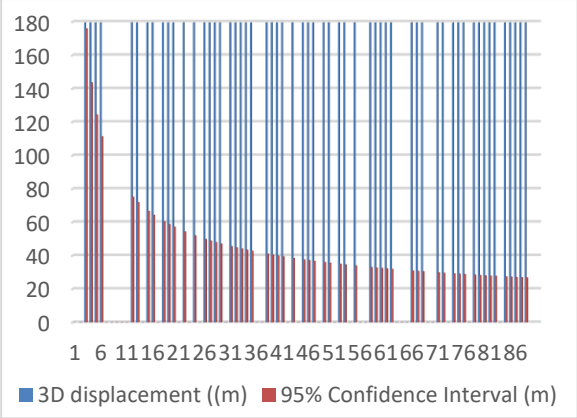

Fig. 6 3D Displacement and their respective Confidence 1ntervals for Prism 2

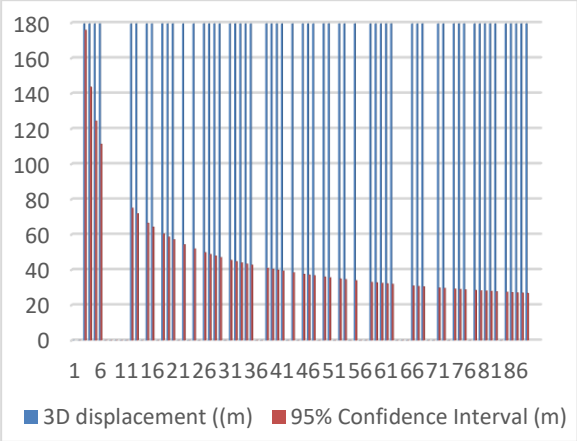

Fig. 7 3D Displacement and their respective Confidence 1ntervals for Prism 3

4.2 AI Models Developed

In developing the various AI models, several architectures were exploited. The essence was to determine the most efficient architecture for each AI technique. Subsequently, the same set of training and testing data were used to train and evaluate all the developed AI models, and the best-performing architecture for each method was selected. The results obtained by the best architectures are presented in the subsequent sub-sections.

4.2.1 PRIM Model

The adjustable parameters of the PRIM model were alpha peel, alpha paste, min support, max boxes, and terminate below mean. The best-performing architecture for the PRIM model had an alpha peel, alpha paste min support, max boxes, and terminate below mean values of 0.2, 0.1, 0.1, inf, and 1, respectively. Tables 1 to 3 present the statistical performances of the PRIM model in predicting pit wall deformation for Prisms 1, 2 and 3.

The statistical results in Tables 1, 2 and 3 indicate that the PRIM model performed reasonably when used to predict pit wall deformation for Prisms 1 and 2. This assertion is confirmed by the training and testing results where lower MSE, RMSE, and MAE values and relatively high R^2 values were recorded. For Prism 3, the PRIM model's performance was less satisfactory in both training and testing. This was because higher MSE, RMSE and MAE values and lower R^2 values were produced by the model, indicating that it struggled to capture the deformation patterns of the data effectively.

Table 1 Performance of PRIM Model on Prism 1

Evaluation Metric	PRISM 1	
	Train	Test
MSE	0.354176	0.943961
RMSE	0.595127	0.971577
MAE	0.334634	0.595918
R^2	0.834996	0.71254

Table 2 Performance of PRIM Model on Prism 2

Evaluation Metric	PRISM 2	
	Train	Test
MSE	0.634726	0.458847
RMSE	0.796697	0.677382
MAE	0.462776	0.422292
R^2	0.655404	0.76072

Table 3 Performance of PRIM Model on Prism 3

Evaluation Metric	PRISM 3	
	Train	Test
MSE	3.775537	1.332795
RMSE	1.943074	1.154467
MAE	0.826691	0.749227
R^2	0.409614	0.671484

4.2.2 RBFNN Model

The RBFNN model required changing various parameters, such as the number of neurons and width parameter, to achieve the optimum structure for the best prediction output. For this study, the optimum structure of the RBFNN model for Prism 1 was [3-20-1] with a width parameter value of 2.11. This indicates three (3) inputs which were the (E, N, and Z), twenty (20) hidden neurons, and one (1) output (D), representing the predicted deformation or displacement. For Prism 2, the optimum RBFNN model was [3-20-1] with a width parameter value of 1.1. Similarly, the RBFNN model for Prism 3 was [3-20-1] with a width parameter value of 2.6. Tables 4 to 6 summarise the statistical results obtained by the

model for the training and test samples on the three prisms.

The RBFNN model demonstrates remarkable predictive performance for all three prisms. This means that the models effectively captured the functional relationship between the input variables and the deformation. Moreover, the RBFNN models' ability to generalise is evident from the consistency in performance between the training and testing datasets for each prism. For Prisms 2 and 3, the models achieved a near-perfect fit to the data, as indicated by the very high R^2 and low MSE, RMSE, and MAE values. These results suggest that the RBFNN is well-suited for predicting pit wall deformation or displacement because it can provide accurate estimates even when the input-output mapping relationship is highly nonlinear.

Table 4 Performance of RBFNN Model on Prism 1

Evaluation Metric	PRISM 1	
	Train	Test
MSE	0.374843	0.380707
RMSE	0.612244	0.617014
MAE	0.275925	0.375651
R^2	0.825368	0.884065

Table 5 Performance of RBFNN Model on Prism 2

Evaluation Metric	PRISM 2	
	Train	Test
MSE	0.000976	0.004553
RMSE	0.031242	0.067478
MAE	0.013981	0.037409
R^2	0.99947	0.997626

Table 6 Performance of RBFNN Model on Prism 3

Evaluation Metric	PRISM 3	
	Training	**Testing**
MSE	0.0002	0.0002
RMSE	0.0137	0.0130
MAPE	0.0657	0.0580
MAE	0.0034	2.798E-06
R^2	0.99997	0.999960

4.2.3 BPNN

The optimum BPNN model structure for Prism 1 comprised three (3) input variables, eighty-six (86) neurons in a single hidden layer, and one (1) output, as such having a structure of [3-86-1]. For Prism 2, the BPNN model had [3-19-1] that is, three inputs, nineteen hidden neurons and one output. For Prism 3, the optimum BPNN model was three inputs, sixteen hidden neurons and one output with designated structure of [3-16-1]. In all the BPNN models for Prisms 1, 2 and 3, the hyperbolic tangent activation function was used in the hidden layer of the model, while the linear function was used to activate the output layer. These functions enabled the model to capture the non-linearity and linearity measures associated with the input and output data. The Levenberg Marquardt backpropagation algorithm was adopted for training the model. The predictive performances of the BPNN models for each Prism are given in Tables 7 to 9.

The BPNN models consistently demonstrate strong predictive performance across all prisms. They exhibit low error metrics (MSE, RMSE, MAE) and high R^2 values, indicating the closeness of the predicted displacement values to the actual. Thus, based on Table 7, it is evident that the BPNN model demonstrates strong performance with a low MSE and RMSE, indicating that it effectively predicts pit wall deformation. The MAE is also relatively small, signifying accurate predictions. The high R^2 value close to 1 indicates that the model explains a large portion of the variance in the data. Similar to the results obtained for Prism 1, the BPNN model for Prism 2 exhibits excellent predictive performance, as depicted in Table 8. The MSE, RMSE, and MAE are all low, suggesting accurate predictions. The R^2 value close to 1 indicates a strong fit between predicted and actual values. Table 9 indicates that the BPNN model attained the best result for Prism 3, accomplishing extremely low MSE, RMSE, and MAE scores, indicating very accurate predictions. The R^2 value close to 1 suggests an excellent fit for this model.

Table 7 Performance of BPNN Model on Prism 1

Evaluation Metric	PRISM 1	
	Train	Test
MSE	0.382024	0.315396
RMSE	0.618081	0.561601
MAE	0.291905	0.365702
R^2	0.822022	0.903954

Table 8 Performance of BPNN Model on Prism 2

Evaluation Metric	PRISM 2	
	Train	**Test**
MSE	0.024348	0.025248
RMSE	0.156039	0.158895
MAE	0.04028	0.050845
R^2	0.986781	0.986834

Table 9 Performance of BPNN Model on Prism 3

Evaluation Metric	PRISM 3	
	Training	Testing
MSE	0.0008	0.0002
RMSE	0.0291	0.0140
MAPE	0.0011	0.0011
MAE	0.0008	1.1020E-05
R^2	0.9999	0.99995

4.2.4 GMDH Model

Since the GMDH model comprises active and self-organised neurons, the networks can automatically calculate the most crucial input variables, including the number of layers, the number of neurons in hidden layers, and the ideal model structure. As such, it is unnecessary to exploit various architectures to obtain the most efficient. Table 10 presents the final models of the GMDH for predicting the deformation for each prism.

Table 10 GMDH Optimum Prediction Models for Prisms 1, 2 and 3.

Prism	Layer Number	No. of Neurons	Generated Model Equations
1	1	1	$x4 = -1511517214.75–(2418.78726839\times N) + (9816.93181812\times E) + (0.0479923852483\times E\times N) +(0.012431403085\times N^2)-0.0961275630212(E^2)$
	2	2	$x7 = 775989.982992 –(159560.888474\times x4) – (4.63241866654\times E) + (1.27531411177\times E\times x4) + (0.00119597414548\times x4^2)- (1.25465852756\times 10^{-5} \times E^2)$ $x8 = 10061.0057313 –(2285.2729981\times x4) + (0.0501895605002\times N) + 0.00873857302548\times N\times x4) + (0.00117732363721\times x42) – (3.38961659877\times 10^{-07}\times N^2)$
	3	1	$x10 = -0.933088514069–(21.1071150389\times x8) + (22.6791958936\times x7) + (981.152368054\times x7\times x8) – (487.658948988\times x8^2)-493.56434846\times x7^2)$
	4	1	$Model = -25214.8002185 + (5090.96826363\times x10) + (16.7995429237\times Z) – (4.21516195138\times Z^*x10) – (0.0379030064304\times x10^2) + (0.0033809003734\times Z^3)$
2	1	3	$x4 = 138291193.494 + (25.4845581055\times N) – (7372.27298846\times E) + (0.0029577019824\times E\times N) – (0.00202893848265\times N^2) + (0.0523463932664\times E^2)$ $x5 = 20854980.7672 – (13678.466942\times Z) + (699.026611692\times E) + (0.154271700416\times E\times Z) – (2.15533914835\times Z^2) – (0.00715234385189\times E^2)$ $x6 = 5908325.29719 – (1432.58163579\times Z) – (47.0961007853\times N) + (0.109885277754\times N\times Z) – (11.1138665406\times Z^2) – (0.000151440966832\times E^2)$
	2	2	$x7 = -53.941703589 + (30.8563220732\times x5) + (1.54713180637\times x4) – (0.530899121309\times x4\times x5) – (3.7540562418\times x5^2) – (0.00369077043192\times x4^2)$ $x8 = 586.730487607 – (354.787846236\times x6) + (13.903706616\times x5) – (3.46554856355\times x5\times x6) + (49.7699825656\times x6^2) + (0.257894086767\times x5^2)$
	3	1	$Model = -0.122352293817 – (1.26478575791\times x8) + (1.56380103002\times x7) –(3.15420232287\times x7\times x8) + (2.01091370213\times x8^2) + (1.29019188683\times x7^2)$

3	1	2	x4 = 15276512.844 – (39.2004850073*N) – (199.052114098×E) + (0.000294601897375×E×N) + (0.0009437689656×N^2) – (0.00346690510599×E^2) x5 = -723088470.972 – (210562.645858×Z) + (6858.41309688×E) + (2.16344867169×E×Z) – (25.5372534698×Z^2) – (0.0109059435517×E^2)
	2	1	x7 = -7.51797436666 + (0.201321376032×x5) + (2.28286407323×x4) – (0.0057344339419×x4×x5) + (0.0072903619418×$x5^2$) – (0.0373285429086×$x4^2$)
	3	1	Deformation = 436589.145983 – (163253.227121×x7) – (68.1088450012×Z) + (135.272830425×Z×x7) + (0.00214540054163×$x7^2$) – (0.243319024281×$x3^2$)

The statistical performance results are presented in Tables 11 to 13.

As presented in Table 11, The GMDH model demonstrates reasonably good predictive performance on Prism 1. The MSE is relatively low, indicating decent predictive accuracy. The RMSE and MAE values, while not as low as desired, suggest acceptable prediction errors. The R^2 value is relatively high, indicating that the model explains a significant portion of the variance and captures some of the underlying patterns in Prism 1 data. For Prism 2 (Table 12), the GMDH achieved a relatively low MSE, RMSE and MAE values, suggesting lower prediction errors. The R^2 value is higher, indicating that the model could explain the variance in Prism 2 data effectively. For Prism 3, presented in Table 13, the GMDH model exhibited a decent predictive accuracy. This is evident in the respective RMSE, MAE and R^2 values obtained.

Table 10 Performance of GMDH Model on Prism 1

Evaluation Metric	PRISM 1	
	Training	Testing
MSE	0.0146	0.0407
RMSE	0.1207	0.2017
MAPE	0.4628	0.4628
MAE	0.0046	0.0156
R^2	0.9932	0.9879

Table 11 Performance of GMDH Model on Prism 2

Evaluation Metric	PRISM 2	
	Train	Test
MSE	0.15142	0.096625
RMSE	0.389128	0.31085
MAE	0.202848	0.150665
R^2	0.917793	0.958

Table 12 Performance of GMDH Model on Prism 3

Evaluation Metric	GMDH	
	Train	Test
MSE	0.042185	0.047691
RMSE	0.20539	0.218382
MAE	0.101552	0.101277
R^2	0.993403	0.988245

4.3 Statistical Evaluation of the Developed AI Models

A comparative evaluation was performed to gain crucial insights into the various developed models' performance. All the models were evaluated with the same test dataset to avoid bias. The resulting statistical outcomes are discussed in the subsequent subheadings.

4.3.1 Statistical Evaluation of Models for Prism 1

Based on Table 14, the PRIM model shows moderate performance in terms of MSE (0.943961), RMSE (0.971577), and MAE (0.595918), indicating low level of accuracy in predicting pit wall deformation. However, the R^2 value of 0.71254 suggests that it explains only a moderate amount of variance in the data. The RBFNN model outperforms PRIM with significantly lower MSE (0.380707), RMSE (0.617014), and MAE (0.375651) values. The R^2 value of 0.884065 attained by the BPNN model indicates a strong fit between predicted and actual deformation values. The GMDH model also showed strong performance with a remarkably low MSE (0.040697) and RMSE (0.201736). The MAE score of 0.10554 is also quite low, signifying accurate predictions. The R^2 value of 0.987607 indicates an excellent fit, making GMDH a competitive choice. Regardless, the BPNN model exhibits the best performance among these three models for Prism 1. The reason is that the BPNN

achieved the lowest MSE (0.315396), RMSE (0.561601), and MAE (0.365702) scores, indicating a marginal variation between the predicted and actual deformation. This assertion is in line with the R^2 value of 0.903954 which suggests an excellent fit by the BPNN model.

Table 13 Statistical Evaluation of Models on Prism 1 for the Testing Data

AI Model	Evaluation Metrics			
	MSE	**RMSE**	**MAE**	**R^2**
PRIM	0.943961	0.971577	0.595918	0.71254
RBFNN	0.380707	0.617014	0.375651	0.884065
BPPN	0.315396	0.561601	0.365702	0.903954
GMDH	0.040697	0.201736	0.10554	0.987607

4.3.2 Statistical Evaluation of Models for Prism 2

Table 15 indicates that the PRIM model had a moderate performance, with relatively high MSE (0.458847), RMSE (0.677382), and MAE (0.422292) values. The R^2 value of 0.76072 suggests that it could explain about 76.072% of the variation in the displacement when the input variables (E, N and Z) changes. The RBFNN model significantly outperformed PRIM, with very low MSE (0.004553), RMSE (0.067478), and MAE (0.037409) scores. RBFNN's high R^2 value of 0.997626 indicates an almost perfect fit, demonstrating its accuracy in predicting pit wall deformation. On the contrary, the GMDH model exhibits variable performance with MSE (0.096625), RMSE (0.31085), MAE (0.150665) and R^2 (0.958) values better than only the PRIM. Overall, the RBFNN was the better model for predicting deformation for Prism 2 which was followed by BPNN.

Table 14 Statistical Evaluation of Models on Prism 2 for the Testing Data

AI Model	**Evaluation Metrics**			
	MSE	**RMSE**	**MAE**	**R^2**
PRIM	0.458847	0.677382	0.422292	0.76072
RBFNN	0.004553	0.067478	0.037409	0.997626
BPPN	0.025248	0.158895	0.050845	0.986834
GMDH	0.096625	0.31085	0.150665	0.958

4.3.3 Statistical Evaluation of Models for Prism 3

As shown in Table 16, the GDMH model showed strong performance with low MSE (0.047691), RMSE (0.218382), MAE (0.101277) and R^2 value of 0.988245. The interpretation here is that the GMDH could produce predictions that has a marginal variation of 1.1755%. This can be confirmed from the R^2(0.988245) value obtained. However, closely related values were achieved for the BPNN and RBFNN, indicating outstanding predictive capabilities. The PRIM had the worst performance among all the candidate models evaluated for Prism 3.

Table 15 Statistical Evaluation of Models on Prism 3 for the Testing Data

AI Model	**Evaluation Metrics**			
	MSE	**RMSE**	**MAE**	**R^2**
PRIM	1.332795	1.154467	0.749227	0.671484
RBFNN	0.000168	0.012954	0.005512	0.999959
BPPN	0.000196	0.013993	0.005096	0.999952
GMDH	0.047691	0.218382	0.101277	0.988245

In general, the comparative assessment divulges that, overall, the BPNN and RBFNN models consistently demonstrate strong predictive performance across all the three prisms. The BPNN and RBFNN exhibited low error metrics (MSE, RMSE, MAE) and high R^2 values, indicating stronger learning ability and good generalisation performance of these models to capture the relationship between input and output variables effectively. GMDH, while competitive, has shown mixed results across different prisms, and PRIM generally performed moderately compared to the other models.

5 Conclusions

This study proposes utilising AI techniques for estimating pit wall deformation in an open-cast mine. Four AI models, namely, the PRIM, RBFNN, BPNN, and GMDH, were developed. To achieve the best performance, each AI model was meticulously fine-tuned, and their associated parameters were optimised.

The findings of this study encourage the adoption and utilisation of RBFNN and BPNN for pit wall deformation prediction in open-cast mining operations. These models exhibited exceptional accuracy and robust predictive capabilities, providing valuable tools for enhancing safety and operational efficiency in mining. GMDH, with its respectable performance, can serve as an alternative in situations where a balance between accuracy and computational efficiency is sought. However, PRIM, due to its significant errors, may not be the optimal choice for accurate deformation estimation in this context. It can also be stated for an AI model to perform with high order of predictive accuracy, there is the need for continuous model adaptation based on new dataset.

References

Apraku, E. K., Ziggah, Y., Y., Kumi-Boateng, B., (2022), "Accuracy Assessment of Artificial Neural Networks as Viable Techniques for Predicting Open Pit Mine Wall Deformation", Proceeding of the 7th UMaT Biennial International Mining and Mineral Conference, Tarkwa, Ghana, pp. 1-9.

Amiri, M. and Soleimani, S. (2021), "ML-based group method of data handling: an improvement on the conventional GMDH", *Complex and Intelligent Systems*, Springer International Publishing, Vol. 7, No. 6, pp. 2949–2960.

Arthur, C.K., Temeng, V.A., Ziggah, Y. Y., (2019), "Soft computing-based technique as a predictive tool to estimate blast-induced ground vibration", *Journal of Sustainable Mining,* Vol. 18, Issue 4, pp. 287-296.

Bird, B. (2009), "Analysis of Survey Point Displacements Using Total Station Measurements", *Published BSc. Technical Report of the Department of Geomatics Engineering*, British Columbia Institute of Technology, 181 pp.

Bowker, N. L., Chambers, M. D., (2015), "The Risk Public Liability and Economics of Tailings Facility Failures", www.Researchgate.net/publications/283321865. Accessed: 25/08/2022.

Cheng, J. and Xiong, Y., (2017), "Application of extreme learning machine combination model for dam displacement prediction", *Procedia Computer Science*, Vol. 107, pp.373-378.

Dong, M., Wu, H., Hu, H., Azzam, R., Zhang, L., Zheng, Z., Gong, X., (2020), "Deformation Prediction of Unstable Slopes Based on Real-Time Monitoring and Deep AR Mode", SENSORS, Vol. 21, No. 1, pp 14.

Du, J., Yin, K. and Lacasse, S., (2013), "Displacement prediction in colluvial landslides, three Gorges reservoir", *China Landslides*, Vol.10, pp. 203-218.

Duddu, V. R., Pulugurtha, S. S., Mane, A. S. and Godfrey, C. (2020), "Back-propagation neural network model to predict visibility at a road link-level", *Transportation Research Interdisciplinary Perspectives*, The Author(s), Vol. 8, pp. 1–9.

Gourine, B., Mahi, H., Khoudiri, A., and Laksari, Y., (2012), "The GRNN and the RBF Neural Networks for 2D Displacement Field Modelling. Case study: GPS Auscultation Network of LNG reservoir GL4/Z industrial complex–Arzew", Algeria. *Rome, Italy*, pp.6-10.

Huang, C., Xia, H., and Hu, J., (2019), "Surface Deformation Monitoring in Coal Mine Area Based on PSI" *IEEE Access Journal*, Vol. 7, pp. 29672-29678.

Jia, H., Liang, S., Lou, S. and Sheng, X., (2019), "A **k** -Nearest Neighbor Algorithm-Based Near Category Support Vector Machine Method forEvent Identification of **φ** –OTDR", *IEEE Sensors Journal*, Vol. 19, No. 10, pp.3683-3689.

Kalkan E. and Chopra A. K., (2010), "Practical Guidelines to Select and Scale Earthquake Records for Nonlinear Response History Analysis of Structures", *U.S. Geological Survey Open-File Report*, pp. 127.

Kutterer, H., Alkhatib, H., Paffenholz, J. A. and Vennegeerts, H., (2010), "Monte-Carlo simulation of profile scans from kinematic TLS", In *Proceedings of the FIG Congress* (p. 12).

Li, Z., Goebel, K. and Wu, D., (2019), "Degradation modeling and remaining useful life prediction of aircraft engines using ensemble learning", *Journal of Engineering for Gas Turbines and Power*, Vol.*141*, *No.*4, pp. 041008.

Miima, J.B., and Niemeier, W., (2004), "Adapting neural networks for modelling structural behavior in geodetic deformation monitoring", *ZfV-Zeitschrift für Geodäsie, Geoinformation und Land management*, Vol. 129, No. 3, pp. 160-167.

Miao, F., Wu, Y., Xie, Y. and Li, Y., (2018)," Prediction of landslide displacement with step-like behavior based on multialgorithm optimization and a support vector regression model", *Landslides*, Vol.*15*, pp.475-488.

Mostajeran, F. and Hosseini, S. M. (2023), "Radial basis function neural network (RBFNN)

approximation of Cauchy inverse problems of the Laplace equation", *Computers and Mathematics with Applications*, Vol. 141, pp. 129–144.

Negnevitsky, M., (2005), *Artificial intelligence a guide to intelligent systems*, Addison Wesley Publishers, Harlow-England, 610pp.

Okiemute, E. S., Nnonyelu, O. M, and Fatai, O. O., (2018), "Monitoring and Analysis of Vertical and Horizontal Deformations of a Large Structure Using Conventional Geodetic Techniques", *Journal of Environment and Earth Science*, Vol. 12, No. 8, pp. 52 -61.

Osasan, K. S., and Afeni, T. B., (2010), "Review of surface mine slope monitoring techniques", *Journal of Mining Science*, Vol. 46, pp.177-186.

Russell, S. and Norvig, P., (2003), *Artificial intelligence – a modern approach*, Pearson Higher Education, Upper Saddle River, New Jersey, 1095pp.

Samantaray, S. and Sahoo, A. (2020), "Prediction of runoff using BPNN, FFBPNN, CFBPNN algorithm in arid watershed: A case study", *International Journal of Knowledge-Based and Intelligent Engineering Systems*, Vol. 24, No. 3, pp. 243–251.

Srinivasan, D., (2008), "Energy demand prediction using GMDH networks", *Neurocomputing*, Vol.72, Issues 1-3, pp. 625-629.

Sunwen, D., Feng, G., Wang, J., Feng, S., Malekian, R. and Li, Z., (2019), "A New Machine Learning Prediction Model for Slope Deformation of an Open-Pit Mine: An Evaluation of Field Data", *Energies*, Vol. 12, No. 7, pp. 1 – 14.

Xu, X. Z., Ding, S. F., Shi, Z. Z. and Zhu, H. (2012), "Optimizing radial basis function neural network based on rough sets and affinity propagation clustering algorithm", *Journal of Zhejiang University: Science C*, Vol. 13, No. 2, pp. 131–138.

Xu, Y. and Qiu, T. T., (2021), "Human activity recognition and embedded application based on convolutional neural network", *Journal of Artificial Intelligence and Technology*, Vol.1, No. 1, pp.51-60.

Yakubu, I., Ziggah, Y.Y., Baafi, K. A., (2018), "Prediction of Tidal Effect in Crustal Deformation Monitoring: A Geodetic Perspective" *Ghana Journal of Technology*, Vol. 2, No. 2, pp. 63 – 69.

Zhou, W., Zhang, W., Yang, X. and Wu, W., (2021), "An improved GNSS and InSAR fusion method for monitoring the 3D deformation of a mining area", *IEEE Access*, Vol.9, pp.155839-155850.

Zhang, H., Zhou, J., Jahed Armaghani, D., Tahir, M.M., Pham, B.T. and Huynh, V.V., (2020), "A combination of feature selection and random forest techniques to solve a problem related to blast-induced ground vibration", *Applied Sciences*, Vol. *10, No.* 3, 869pp.

Zhang, Z., Fei, S. and Xing, L., (2017), "Analysis on the Influence of Adjacent Double Foundation Pit Excavation on Tunnel Deformations", *Journal of University of Shanghai for Science & Technology*, Vol. 39, No. 2, pp.176-181

Zhu, Y., Xu, J. and Zhang, S. (2021), "Application of Optimized GA-BPNN Algorithm in English Teaching Quality Evaluation System", *Computational Intelligence and Neuroscience*, Vol. 2021, pp. 1–9.

Authors

Yakubu Issaka is an Associate Professor of Geomatic Engineering and a Consulting Engineer currently working at University of Mines and Technology, Tarkwa-Ghana. He holds BSc degree in Geomatic Engineering from KNUST, Kumasi-Ghana, MPhil and PhD in Geomatic Engineering from the (UMaT), Tarkwa-Ghana. He holds an MSc in Land Policy and Administration from the University of Cape Coast. He also has a Certificate in Disaster Risk Management and Environmental Assessment for Spatial Planning from the ITC-University of Twente, The Netherlands. He is involved in the broad areas of Geomatic Engineering applications research.

Yao Yevenyo Ziggah is a Senior Lecturer at the Geomatic Engineering Department of the University of Mines and Technology (UMaT). He holds a BSc in Geomatic Engineering from UMaT, Meng and PhD in Geodesy and Survey Engineering from China University of Geosciences (Wuhan). He is a member of the International Association of Geodesy (IAG), the International Association of Mathematical Geosciences (IAMG), the Institute of Mining, Metallurgy and Petroleum (WAIMM) and the International Association of Engineers (IAENG). His research interests include the application of artificial intelligence in engineering and geoscience, 2D/3D coordinate transformation, geodetic deformation modelling, geoid modelling and height systems.

Frank Osei. is a postgraduate student of Geomatic Frank Osei. is a postgraduate student of Geomatic Engineering at the University of Mines and Technology, Tarkwa, Ghana. He holds a three-year Professional Diploma in Mine Surveying from the Kwame Nkrumah University of Science and Technology, School of Mines Tarkwa, Ghana. He is a highly experienced professional Surveyor with a distinguished career spanning over two decades. With a robust background in the mining, exploration, civil and construction industries. He is a trusted expert in his field, known for his precision, dedication and innovative approach to Surveying. His research interests include Mine and Engineering Surveying. He is a member of the Institution of Surveyors (GhIS).